


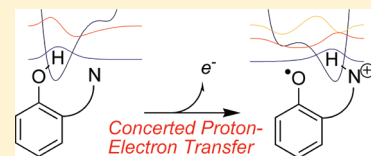
# Probing Quantum and Dynamic Effects in Concerted Proton–Electron Transfer Reactions of Phenol–Base Compounds

Todd F. Markle,<sup>\*,†</sup> Adam L. Tenderholt, and James M. Mayer<sup>\*</sup>

Department of Chemistry, University of Washington, Box 351700, Seattle, Washington 98195-1700, United States

 Supporting Information

**ABSTRACT:** The oxidation of three phenols, which contain an intramolecular hydrogen bond to a pendent pyridine or amine group, has been shown, in a previous experimental study, to undergo concerted proton–electron transfer (CPET). In this reaction, the electron is transferred to an outer-sphere oxidant, and the proton is transferred from the oxygen to nitrogen atom. In the present study, this reaction is studied computationally using a version of Hammes-Schiffer’s multistate continuum theory where CPET is formulated as a transmission frequency between neutral and cation vibrational-electronic states. The neutral and cation proton vibrational wave functions are computed from one-dimensional potential energy surfaces (PESs) for the transferring proton in a fixed heavy atom framework. The overlap integrals for these neutral/cation wave functions, considering several initial (i.e., neutral) and final (i.e., cation) vibrational states, are used to evaluate the relative rates of oxidation. The analysis is extended to heavy atom configurations with various proton donor–acceptor (i.e., O–N) distances to assess the importance of heavy atom “gating”. Such changes in  $d_{\text{ON}}$  dramatically affect the nature of the proton PESs and wave functions. Surprisingly, the most reactive configurations have similar donor–acceptor distances despite the large ( $\sim 0.2$  Å) differences in the optimized structures. These theoretical results qualitatively reproduce the experimental faster reactivity of the reaction of the pyridyl derivative **1** versus the  $\text{CH}_2$ –pyridyl **2**, but the computed factor of 5 is smaller than the experimental  $10^2$ . The amine derivative is calculated to react similarly to **1**, which does not agree with the experiments, likely due to some of the simplifying assumptions made in applying the theory. The computed kinetic isotope effects (KIEs) and their temperature dependence are in agreement with experimental results.



## INTRODUCTION

Redox processes that occur with changes in proton content, proton-coupled electron transfer (PCET), are of increasing interest from biological chemistry to the energy sciences.<sup>1</sup> PCET processes can occur via a series of simple electron transfer (ET) and proton transfer (PT) steps. Alternatively, the proton and electron can be transferred in a single kinetic step, as concerted proton–electron transfer (CPET).<sup>2</sup> An example of CPET from biology that has received considerable attention is the oxidation of tyrosine-Z to yield a neutral tyrosyl radical in the Kok S-state mechanism of Photosystem II. Here, the electron is transferred to the chlorophyll radical cation  $\text{P}_{680}^+$ , and the proton is transferred across a hydrogen bond to a nearby histidine residue.<sup>3</sup> While the loss of a proton and electron is a net hydrogen atom transfer from the tyrosine, here the oxidant and basic sites are chemically distinct, an example of separated CPET.<sup>1</sup>

A number of laboratories have used small-molecule phenol model systems to study separated CPET.<sup>4–9</sup> Our own efforts have focused on oxidations of phenols bearing an intramolecular hydrogen bond to basic moieties (Scheme 1).<sup>10–12</sup> In this system, chemical or electrochemical oxidation of the phenol is coupled to intramolecular PT, yielding the formally distonic radical cation.<sup>10–13</sup> The CPET mechanism is indicated in these oxidations by thermochemical arguments, the observation of primary, although moderate,  $k_{\text{H}}/k_{\text{D}}$  kinetic isotope effects (KIE), and the variation of rates with driving force ( $\Delta\Delta G^\ddagger/\Delta\Delta G^\circ_{\text{CPET}} \approx 0.5$ ).<sup>10–12</sup>

Changing the base in these phenol–base compounds provides insight into the parameters that control CPET reactivity, as these

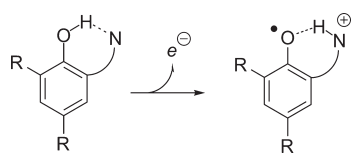
molecules have relatively well-defined proton transfer coordinates. In a study of nine variously substituted phenol-imidazoles, we found that  $\Delta G^\circ$  is the primary determinant of CPET rate constants despite moderate changes in structure and hydrogen bonding.<sup>11</sup> The proton donor–acceptor distance  $\text{O} \cdots \text{N}$  in these molecules, termed  $R$ , varies in the solid state from 2.53 to 2.65 Å (by X-ray crystallography). Changes in the nature of the hydrogen bond are indicated via the phenolic proton chemical shift ( $\delta$  11.6–13.7 ppm) or calculated O–H stretching frequency ( $\nu_{\text{OH}}$ , 2996–3130  $\text{cm}^{-1}$ ).<sup>11</sup> In contrast, we found phenol–base compounds that bear 2'-pyridyl (**1**, Scheme 2) or 2'-imidazolyl moieties react with bimolecular rate constants up to 2 orders of magnitude faster than the phenol–amine compound **3** at the same driving force and with similar oxidants.<sup>10</sup> Inserting a methylene unit between the phenol and pyridine rings substantially decreases the reactivity toward CPET, with compound **2** reacting much more slowly than **1**, at rates comparable to those of **3**.<sup>12</sup> That study concluded that the increased rates observed for **1** and, by extension, the phenol–imidazolyl compounds result from their stronger hydrogen bonds, a consequence of the conjugated  $\pi$  system linking the proton donor and acceptor. This report describes computational analyses of these CPET processes using a nonadiabatic quantum CPET theory, to provide insight into the

Received: September 22, 2011

Revised: December 5, 2011

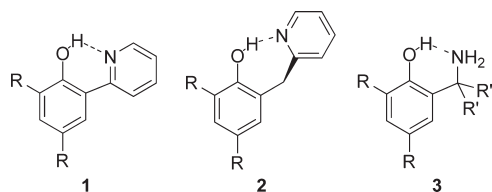
Published: December 07, 2011

### Scheme 1. Separated CPET in the Oxidation of Phenol–Base Compounds<sup>a</sup>



<sup>a</sup> N = basic moiety.

### Scheme 2. Phenol–Base Compounds<sup>a</sup>



<sup>a</sup> In this computational study, R = R' = methyl; in the previous experimental studies, R = *tert*-butyl, R' = phenyl.<sup>10–12</sup>

origins of the substantial difference in reactivity among the phenol–base compounds 1–3.

Outer-sphere electron transfer is well understood in the framework of Marcus theory.<sup>14</sup> The product and reactant surfaces are treated as diabatic parabolas, where the rate constant is given by

$$k = \frac{2\pi}{\hbar} |V_{\text{ET}}|^2 (4\pi\lambda k_{\text{B}}T)^{-1/2} \exp\left(\frac{-(\Delta G^\circ + \lambda)^2}{4\lambda k_{\text{B}}T}\right) \quad (1)$$

where  $\Delta G^\circ$  is the thermodynamic driving force,  $\lambda$  is the reorganization energy required to move solute and solvent nuclei to the geometry of the product without transfer of the electron,  $V_{\text{ET}}$  is the matrix element that describes the coupling between the two diabatic electronic surfaces for reactants and products, and the other constants have their usual meaning.

Most current theories of PT reactivity begin from a Marcus-type model with a quadratic dependence on  $\Delta G^\circ$ . The proton is treated as a quantum mechanical particle, with a Born–Oppenheimer-type separation of the fast proton movement from movement of the heavier nuclei.<sup>15,16</sup> Hammes-Schiffer's multistate continuum theory has been the most influential example.<sup>17,18</sup> It and other approaches continue to be developed.<sup>19</sup> A complete theory of CPET would involve a full quantum dynamical treatment, without Born–Oppenheimer or proton/heavy nuclei separations, but this is not possible for a system of any size.<sup>20</sup> At the other extreme, many CPET reactions are being treated by traditional quantum chemical approaches based on adiabatic transition state theory with a classical proton.<sup>21</sup> We use one form of multistate continuum theory because there is an outer-sphere electron transfer component of these CPET reactions, because CPET is typically considered to be nonadiabatic as discussed below, and because it is informative to have a test case of applying the theory.

In multistate continuum theory, the transferring proton and electron are both treated as quantum particles, and orthogonal PT and ET reaction coordinates are defined by the polar medium. CPET is formulated as transmission between pairs of diabatic proton–electron vibronic states ( $\mu, \nu$ ), with the proton

in vibrational state  $\mu$  for electronic state I and  $\nu$  for electronic state II. CPET rate constants are given by

$$k = \frac{2\pi}{\hbar} \sum_{\mu} P_{\mu}^{\text{I}} \sum_{\nu} \{V_{\mu\nu}\}^2 (4\pi\lambda_{\mu\nu}k_{\text{B}}T)^{-1/2} \exp\left(\frac{-\Delta G_{\mu\nu}^\ddagger}{k_{\text{B}}T}\right) \quad (2)$$

where  $P_{\mu}^{\text{I}}$  is the Boltzmann population of the initial vibrational state,  $V_{\mu\nu}$  is the matrix coupling element for the diabatic surfaces, and the free-energy barrier

$$\Delta G_{\mu\nu}^\ddagger = \frac{(\Delta G_{\mu\nu}^\circ + \lambda_{\mu\nu})^2}{4\lambda_{\mu\nu}} \quad (3)$$

has a Marcus-type dependence.<sup>17</sup> The matrix coupling element  $V_{\mu\nu}$  can be approximated as

$$V_{\mu\nu} \approx V^{\text{el}} \langle \phi_{\mu}^{\text{I}} | \phi_{\mu}^{\text{II}} \rangle = V^{\text{el}} S_{\mu\nu} \quad (4)$$

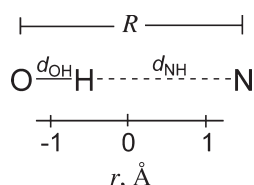
where  $V^{\text{el}}$  is the electronic coupling, and  $S_{\mu\nu}$  is the Franck–Condon overlap of proton wave functions  $\mu$  and  $\nu$ . Because the overall coupling (the weighted double sum of  $S_{\mu\nu}$ ) contains both electronic and vibrational overlaps, it is typically considered to be  $\ll k_{\text{B}}T$ , and therefore most CPET reactions are non-adiabatic.<sup>17,18,22</sup> The relatively localized nature of the proton leads to a strong dependence of  $S_{\mu\nu}$  on the donor–acceptor hydrogen distance  $R$ . Including variation in  $R$  adds another level of complexity as will be described below.<sup>17,23</sup> Hammes-Schiffer and co-workers have used this model to examine a number of CPET systems, including formal hydrogen atom transfer reactions in lipoxxygenase,<sup>24</sup> in phenol/phenoxyl and toluene/benzyl radical couples,<sup>25</sup> and in complexes of Ru, Os, and Fe.<sup>26–29</sup> It has also been used to analyze separated CPET phenol oxidations, model systems for Tyr oxidation.<sup>30–33</sup>

Here, we evaluate the relative importance of factors that define CPET reactivity in the context of multistate continuum theory. Because of the well-defined nature of the system and our focus on relative reactivity, we have been able to apply the theory without any fitted or assigned parameters. It is, however, necessary to apply some simplifications to apply the theory. In that light, this Article makes an interesting contrast with the related study of Johannissen et al. that takes a quite different approach to very similar reactions.<sup>5e,34</sup> The computations reported here probe the factors that contribute to CPET reactivity in the multistate continuum model. Specifically, we examine the overlap factors of proton wave functions, the Boltzmann populations of initial states, and the contributions of pathways to or from vibrational excited states. Molecular configurations with varying proton donor–acceptor distances are considered to model dynamic effects along this coordinate.

## ■ COMPUTATIONAL METHODS

Unless stated otherwise, all calculations were performed using Gaussian 03.<sup>35</sup> All optimized geometries were confirmed to be local minima by harmonic vibrational analysis. DFT calculations utilized the (U)B3LYP functional with 6-31G(d) basis set used for all atoms with the exception of the transferring proton, for which a set of p polarization functions were included, that is, 6-31G(d,p). Inclusion of diffuse or additional polarization basis functions was found to produce no qualitative changes (see the Supporting Information). The phenol–base compounds studied experimentally<sup>10–12</sup> were simplified for computational purposes

**Scheme 3. Important Geometric Parameters Where  $R = d_{\text{ON}}$  and  $r = 1/2(d_{\text{OH}} - d_{\text{NH}})$**



with the *tert*-butyl groups at the 4 and 6 positions in **1–3** and the *gem*-diphenyl groups in **3** replaced by methyl groups (Scheme 2).

All calculations were performed in the gas phase. PCM models of MeCN solvent with  $\epsilon = \epsilon_{\text{op}}$  appear to have relatively minor effects on the shape of the hydrogen-bond potentials for the neutral and cation (see the Supporting Information). Standard self-consistent reaction field models of solvation (e.g., the polarizable continuum model) were developed to compute equilibrium solvation free energies and, not surprisingly, have been shown to substantially overestimate solvent reorganization effects in ET processes.<sup>36</sup>

Each proton transfer potential energy surface (PT-PES) was obtained from a series of partial geometry optimizations in which the proton position is optimized at various points along the PT coordinate,  $r = 1/2(d_{\text{OH}} - d_{\text{NH}})$ , as shown in Scheme 3. The positions of all atoms except for the transferring proton were fixed at approximated transition state structures for the CPET process; see below. With this fixed heavy-atom structure, a set of calculations were done with incremental changes in the O–H or N–H distance (optimizing the proton position given this constraint). The energies of the structures obtained are plotted with respect to the PT coordinate and then fitted to a six-order polynomial describing the PT-PES. Proton vibrational energy levels and wave functions were calculated numerically for these one-dimensional potential energy wells using a basis set of 200 harmonic oscillator functions.<sup>37</sup> The process was repeated with a radical cation wave function, using the same averaged geometry for the remaining atoms. This gives the proton PES for both the neutral and the radical cation states within the same heavy atom framework. Other sets of calculations were done with values of  $R$  (the proton donor–acceptor distance) fixed at various distances. In this case, the structures of the neutral molecule and the cation were optimized with  $R$  fixed at the specified value, these two structures were averaged to give transition structure  $\text{TS}_{R_0}$  and the proton transfer PES was obtained as described above.

## RESULTS AND DISCUSSION

**I. Approach.** CPET reactivity is evaluated in the context of Hammes-Schiffer’s multistate continuum theory (eq 2) to gain insight into the differences in CPET rates observed with **1–3**.<sup>10,12</sup> We begin by noting two experimental observations that allow simplification of this treatment followed by considering the reorganization energy,  $\lambda$ , in more detail.

The first important experimental observation to consider is that these CPET reactions are in the regime where the barrier varies linearly with the overall driving force. The slope is approximately 0.5, that is,  $\Delta\Delta G^\ddagger \cong \Delta\Delta G^\circ/2$ , which implies  $|\Delta G^\circ| \ll \lambda$  for the equations here.<sup>10–12</sup> In this limit, the quadratic form of the Marcus barrier (eq 3) simplifies to the linear equation  $\Delta G_{\mu\nu}^\ddagger = \Delta G_{\mu\nu}^\circ/2 + \lambda_{\mu\nu}/4$ .

Second, the bimolecular rate constants for CPET reactions of **2** and **3** with different chemical oxidants ( $k_{\text{AB}}$ ) are found to follow the Marcus cross relation, that is,  $k_{\text{AB}} = (k_{\text{AA}}k_{\text{BB}}K_{\text{eq}}f)^{1/2}$ , where  $k_{\text{XX}}$  is the rate constant for the degenerate self-exchange reaction  $X + X^+ \rightarrow X^+ + X$ .<sup>10,12</sup> Thus, the intrinsic reactivity of the phenols **1–3** can be described by the rate constant  $k_{\text{AA}}$  for the degenerate self-exchange reaction  $A + A^+ \rightarrow A^+ + A$ . This permits this theoretical treatment to focus on the “half-reaction” self-exchange process, that is,  $A \rightarrow A^+ + e^-$ . For the compounds analyzed here, the CPET half-reaction converts the neutral molecule with the proton bound to the phenoxyl oxygen (**1–3**) to the radical cation with the proton bound to the nitrogen of the base (**1<sup>+</sup>–3<sup>+</sup>**; Scheme 1, right).

The multidimensional seam separating the reactants and products of the degenerate self-exchange reaction must lie symmetrically between **A** and **A<sup>+</sup>** because of the symmetry of the reaction. (In the experimentally measured solution reactions, nonzero values of  $\Delta G^\circ$  will perturb the location of this seam, but the Marcus cross-relation treatment places the intrinsic kinetic information in the self-exchange rate.) We start our analysis below at a fixed geometry  $\text{TS}_0$  that is the average of the neutral and radical cation geometries (Supporting Information). This is the logical starting point because it is the classical transition structure, the crossing point of the neutral and cation surfaces, and analogous to the transition structure in adiabatic electron transfer reactions.<sup>38</sup>  $\text{TS}_0$  is a useful benchmark configuration for comparison with other configurations with different proton donor–acceptor distances.

The intrinsic barrier  $\lambda$  is the energy required to distort the reactants to the structure of the products without transfer of the electron.<sup>14</sup> It has both outer-sphere (solvent) and inner-sphere (solute) contributions (i.e.,  $\lambda = \lambda_{\text{out}} + \lambda_{\text{in}}$ ). The outer-sphere reorganization energy is assumed to be independent of the vibrational state and to be the same for compounds **1–3** because of their similar size and shape. The inner-sphere reorganization energies are 4 times the energy required to take the ground-state reactants to the transition structure in a self-exchange reaction. For simplification of the equations below, we define  $E^* = \lambda_{\text{in}}/4$ .

Equations 2–4 can be simplified significantly when applied to a self-exchange reaction and using these assumptions. When the neutral and cation are in their vibrational ground states ( $\mu = \nu = 0$ ), then  $\Delta G_{00}^\circ = 0$ . For transitions to or from vibrational excited states,  $\Delta G_{\mu\nu}^\circ$  is simply given by the relative vibrational energies, that is:

$$\Delta G_{\mu\nu}^\circ = \epsilon_{\text{rel}-\mu\nu} \equiv (\epsilon_\mu^I - \epsilon_0^I) - (\epsilon_\nu^{\text{II}} - \epsilon_0^{\text{II}}) \quad (5)$$

where  $\epsilon_x$  is the energy of vibrational state  $x$ .

Therefore, these assumptions allow the free energy barrier (eq 3) to be simplified to

$$\Delta G_{\mu\nu}^\ddagger = \frac{\epsilon_{\text{rel}-\mu\nu}}{2} + \frac{\lambda_{\text{out}}}{4} + E^* \quad (6)$$

Combining this equation with the full rate expression (eq 2) and the approximation for the matrix coupling element (eq 4) yields:

$$k = \frac{2\pi}{\hbar} |V^{\text{el}}|^2 (4\pi\lambda k_{\text{B}}T)^{-1/2} \exp\left(\frac{-\lambda_{\text{out}}}{4k_{\text{B}}T}\right) \zeta_0 \quad (7)$$

where all of the terms except  $\zeta_0$  are the same for all three phenols studied here, neglecting the small dependence of the prefactor on



Table 1. Selected Geometrical Parameters for 1–3<sup>a</sup>

	1 <sub>OH</sub>		1 <sup>+</sup> <sub>NH</sub>	2 <sub>OH</sub>		2 <sup>+</sup> <sub>NH</sub>	3 <sub>OH</sub>		3 <sup>+</sup> <sub>NH</sub>
	X-ray <sup>b</sup>	DFT	DFT	X-ray <sup>c</sup>	DFT	DFT	X-ray <sup>b</sup>	DFT	DFT
R(O...N)	2.567(6)	2.564	2.544	2.6914(13)	2.760	2.639	2.58(3)	2.640	2.533
d(O–H)	0.98(5)	1.000	1.623	0.923(17)	0.988	1.644	0.82(3)	0.995	1.549
d(N–H)	1.65(6)	1.653	1.051	1.782(17)	1.806	1.056	1.75(2)	1.743	1.083
d(C1–O)	1.382(4)	1.3455	1.2598	1.3733(13)	1.363	1.268	1.378(3)	1.361	1.272

<sup>a</sup> Distances are in angstroms. The carbons in the phenol ring are numbered such that C1 bears the hydroxyl group. The X-ray structures are for the molecules with R = <sup>t</sup>Bu, R' = Ph; the calculations are for molecules with R = R' = Me (see Scheme 2). <sup>b</sup> Reference 10b; average of the independent molecules in the unit cell (three molecules for 1 and two for 3); errors are standard deviation of these values for independent molecules or thermal ESDs, whichever is larger. <sup>c</sup> Reference 12.

$\lambda_{\text{in}}$ ,  $\zeta_0$  describes the unique electronic–vibronic contributions at TS<sub>0</sub> for the specific phenol, given by

$$\zeta_0 = \sum_{\mu}^{(I)} P_{\mu}^I \sum_{\nu}^{(II)} S_{\mu\nu}^2 \exp\left(\frac{-\epsilon_{\text{rel}-\mu\nu}}{2k_{\text{B}}T}\right) \exp\left(\frac{-E^*}{k_{\text{B}}T}\right) \quad (8)$$

This treatment allows most constants and the outer-sphere reorganization contribution to the rate expression (eq 2) to be separated from the primary effects of a quantum proton, that is, the overlap between the proton wave functions ( $S_{\mu\nu}^2$ ) and the relative vibrational energies that define  $P_{\mu}^I$  and  $\epsilon_{\text{rel}-\mu\nu}$ .

The CPET reactivity at a fixed heavy atom configuration (i.e., TS<sub>0</sub>) can now be computed as a sum over all contributing pathways of initial ( $\mu$ ) and final ( $\nu$ ) proton vibronic states. The next section presents the potential energy surfaces used to calculate these proton states and their wave functions and energies at a fixed heavy atom configuration. These results are then used in section III to evaluate the CPET reactions.

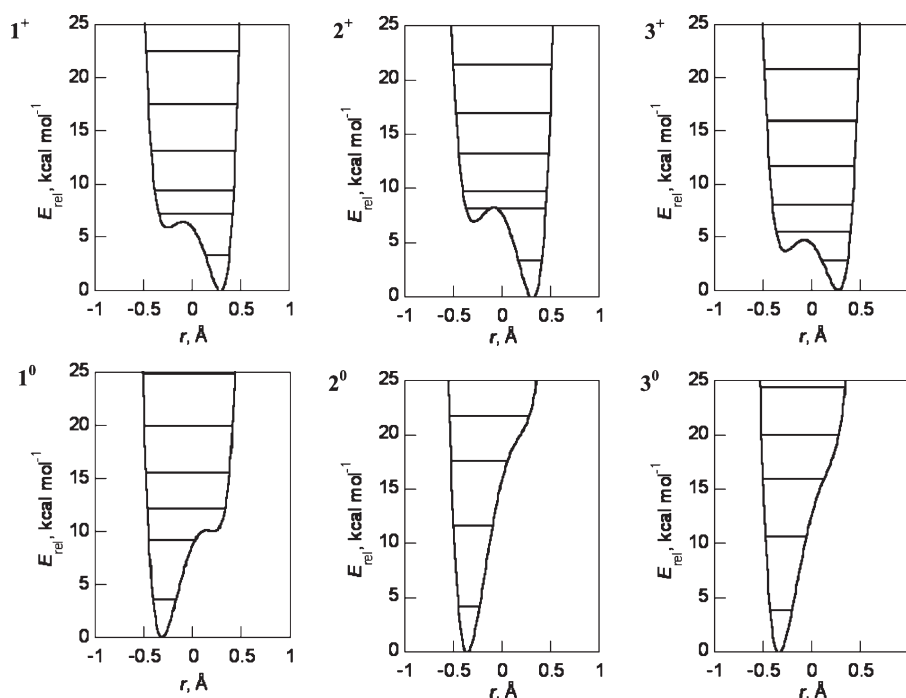
**II. Proton Transfer Potential Energy Surfaces (PT-PESs), Wave Functions, and Energy Levels.** To calculate the proton wave functions and energy levels, the PT-PESs need to be determined. The one-dimensional PT-PESs and wave functions are calculated by assuming a Born–Oppenheimer-type separation of the proton motion from movement of the heavy atoms. This is a reasonable approximation because the proton moves much faster than the heavier atoms.<sup>39</sup> Optimized geometries are determined by gas-phase density functional theory (DFT) calculations, and, as shown by several important geometrical parameters (Table 1), there is good agreement between the calculated forms of neutrals 1–3 (R = R' = Me) and the previously reported crystallographic structures for 1–3 (R = <sup>t</sup>Bu, R' = Ph). Specifically, the important distances involving the donor (O), acceptor (N), and proton are calculated to be within 0.08 Å. The largest deviations are observed for the O–N distances, which are affected by low-energy vibrational modes, and thus are likely susceptible to crystal packing forces. Upon oxidation to the radical cation, the proton transfers to the nitrogen and the phenyl ring have a more quinoidal structure (e.g., the C1–O distance decreases) as is typical of phenoxyl radicals.<sup>40</sup>

The calculated PT-PESs for the neutrals 1<sup>0</sup>–3<sup>0</sup> and the cations 1<sup>+</sup>–3<sup>+</sup> (Figure 1) are quite anharmonic (particularly for the radical cations), which is not surprising for hydrogen-bonded systems,<sup>42</sup> and serve as a reminder that harmonic or Morse potentials should only be employed with caution in CPET computations of strongly hydrogen-bonded systems. These

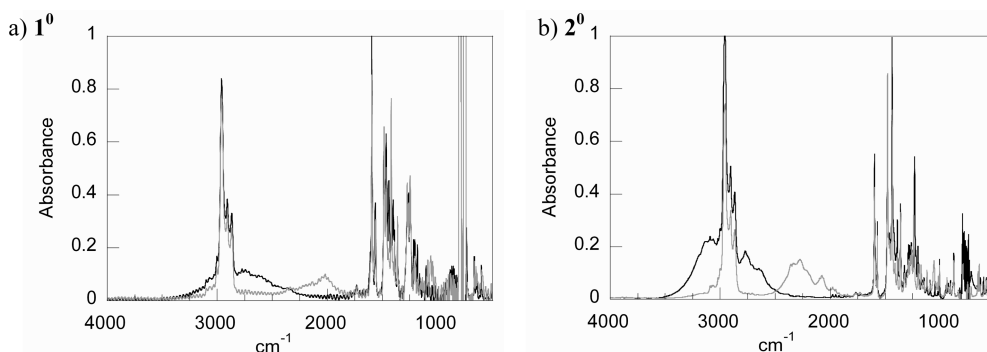
PT-PESs were fitted to sixth-order polynomials, and the vibrational energy levels (indicated by horizontal lines in Figure 1) and wave functions were computed.

There are marked differences in the surfaces of the three systems at their respective TS<sub>0</sub> geometries. In 1<sup>0</sup>, the NH form (termed 1<sup>0</sup><sub>NH</sub>) exists as a minimum 9.8 kcal/mol above the more stable OH form, although the barrier separating them is very small. In contrast, 2<sup>0</sup> and 3<sup>0</sup> have highly asymmetric single-well surfaces with no minima corresponding to the NH forms. In these two surfaces, the “NH form”, if defined as the position of the inflection of the surface, is much higher in energy as compared to 1 (∼21 and ∼17 kcal/mol, above the bottom of the OH well, respectively). The relative stability of 1<sup>0</sup><sub>NH</sub> can be attributed to reduced charge separation due to the electronic conjugation between the oxygen and nitrogen, and the resulting ene-aminone resonance contributor. This leads to a more symmetric energy profile for OH and NH forms, and a strong, resonance-assisted H-bond.<sup>12,39</sup>

Insights into vibrational levels and hydrogen-bond potentials can also be gained from the experimental and computed vibrational spectra. At the optimized ground-state geometry of 1<sup>0</sup>, a standard analytic computation of the normal modes of 1<sup>0</sup> using DFT/B3LYP predicts  $\nu_{\text{OH}} = 3106 \text{ cm}^{-1}$ . Inclusion of anharmonic effects<sup>41</sup> gives  $\nu_{\text{OH}} = 2645 \text{ cm}^{-1}$ . When the proton wave functions are calculated in the diabatic PT-PES with heavy atoms fixed at this optimized ground state, the  $\epsilon_1 - \epsilon_0$  energy gap gives  $\nu_{\text{OH}} = 2313 \text{ cm}^{-1}$ . The differences among these values further indicate the anharmonic nature of the potentials. The experimental IR spectra of such strongly hydrogen-bonded OH systems are known to be quite complex, as a result of anharmonic mixing of modes and dynamical effects, so they do not simply reflect the spacing of the proton vibrational levels.<sup>42</sup> The OH stretching bands observed in the IR spectra of 1<sup>0</sup>–3<sup>0</sup>, as we have noted previously,<sup>12</sup> are very broad, with maxima that are significantly red-shifted as compared to non-hydrogen bonded phenolic OH stretches (∼3600  $\text{cm}^{-1}$ ). For example, 1<sup>0</sup> in CCl<sub>4</sub> solution has a ∼600  $\text{cm}^{-1}$  wide band centered at roughly 2800  $\text{cm}^{-1}$  (Figure 2a), in reasonable agreement with the calculated anharmonic value but not with either the harmonic value or the calculated  $\epsilon_1 - \epsilon_0$  energy gap (3106 and 2313  $\text{cm}^{-1}$ , respectively). Similarly, the broad  $\nu_{\text{OH}}$  band for 2<sup>0</sup> has a complex structure with a maximum at 3090  $\text{cm}^{-1}$  (Figure 2b),<sup>12</sup> in reasonable agreement when anharmonicity is included (3069  $\text{cm}^{-1}$ ) but not within a harmonic approximation (3350  $\text{cm}^{-1}$ ) or for the computed  $\epsilon_1 - \epsilon_0$  energy gap (2616  $\text{cm}^{-1}$ ). For 3<sup>0</sup>,  $\nu_{\text{OH}}$  is 2949  $\text{cm}^{-1}$  from the anharmonic frequency analysis and 2666  $\text{cm}^{-1}$  from the  $\epsilon_1 - \epsilon_0$  energy gap.



**Figure 1.** Proton transfer potential energy surfaces for  $1^0$ – $3^0$  and  $1^+$ – $3^+$ , with heavy atoms frozen at the position of the averaged  $TS_0$ . Horizontal lines indicate the energy levels of the proton vibrational states.



**Figure 2.** Experimental IR spectra ( $CCl_4$  solution) of (a)  $1^0$  and  $1^0$ -d; (b)  $2^0$  and  $2^0$ -d. Spectra of deuterated compounds are in gray. Reprinted with permission from the Supporting Information of ref 12. Copyright 2008 Wiley-VCH.

Returning to the  $TS_0$  geometry relevant to the CPET reactions, the PT-PESs for the cations  $1^+$ – $3^+$  each show a double-well topology, with the NH form being the global minimum (Figure 1). In each case, there is a distinct, albeit shallow, minimum corresponding to the OH form of the radical cation. These OH minima lie above the NH form by 5.9 kcal/mol in  $1^+$ , 6.9 kcal/mol in  $2^+$ , and just 3.8 kcal/mol in  $3^+$ . The difference in energy between the OH and NH forms of the cations is less than the corresponding difference in the neutrals, likely because each form bears a single positive charge. This is compared to the neutral compounds where the NH form is formally zwitterionic and destabilized relative to the OH form. The anharmonic  $O\cdots H-N$  hydrogen bond in  $3_{NH}^+$  is also indicated by the predicted  $\nu_{NH} = 1733\text{ cm}^{-1}$  from anharmonic frequency analyses at the optimized cation geometry and the very low  $\varepsilon_1 - \varepsilon_0 = 935\text{ cm}^{-1}$  (at the  $TS_0$  geometry). The N–H stretching modes

are higher in energy for  $1^+$  and  $2^+$  ( $\varepsilon_1 - \varepsilon_0 = 1352$  and  $1696\text{ cm}^{-1}$  at their respective  $TS_0$  geometries and  $\nu_{NH} = 2541$  and  $2104\text{ cm}^{-1}$  at their optimized cation geometries). The differences in  $\nu_{NH}$  calculated for  $2^+$  and  $3^+$  can be attributed, in part, to the shorter  $r(O-N)$  of  $3^+$  (Table 1).

**III. Analysis of CPET at the  $TS_0$  Geometry.** With the one-dimensional proton vibrational wave functions and their energies at the  $TS_0$  geometry in hand, it is straightforward to evaluate the terms in eq 8: the Franck–Condon factors ( $S_{\mu\nu} = \langle \phi_\mu^I | \phi_\nu^{II} \rangle$ ), the thermal populations of initial states  $\mu$ ,  $P_\mu^I$ , and the energetic terms,  $\exp(-\varepsilon_{rel-\mu\nu}/2k_B T)$ . The sum of all of the individual pathways is  $\zeta_{0,total}$  (eq 8), and the fractional amount that each  $\mu \rightarrow \nu$  pathway ( $\zeta_{0,\mu\nu}$ ) contributes to the overall rate at this  $TS_0$  geometry ( $c_{\mu\nu}^0$ ) is given by eq 9. We emphasize again that this is a preliminary analysis at a single configuration ( $TS_0$ ) neglecting the contribution of donor–acceptor motions, which will be

**Table 2.** Parameters Relevant to CPET Reactivity for the Phenol–Bases at TS<sub>0</sub>

compound	$\zeta_0 (\times 10^{-4})^a$	$E^{*b}$	dominant pathways ( $\mu, \nu$ )			
			(0,0)	(0,1)	(0,2)	(0,3)
1	19	1.6	25%	61%	7%	0%
2	2.0	2.1	6%	60%	33%	1%
3	45	1.7	17%	78%	5%	0%
1d	7.9	1.6	1%	26%	62%	5%
2d	1.0	2.1	0%	3%	84%	12%
3d	27	1.7	1%	63%	32%	3%

<sup>a</sup>From eq 9. <sup>b</sup>Energy required to reach TS<sub>0</sub> from the optimized geometry of the neutral corrected for changes in zero-point energy.

considered in the next section.

$$c_{\mu\nu}^0 \equiv \frac{\zeta_{0,\mu\nu}}{\zeta_{0,\text{total}}} = \frac{P_\mu S_{\mu\nu}^2 e^{-\epsilon_{\text{rel-}\mu\nu}/2k_B T}}{\sum_\mu P_\mu \sum_\nu S_{\mu\nu}^2 e^{-\epsilon_{\text{rel-}\mu\nu}/2k_B T}} \quad (9)$$

For the phenol–pyridine **1** at TS<sub>0</sub>, the dominant pathway for CPET is calculated to occur from the proton vibrational ground state of the neutral reactant to the first excited state of the cation product, with 61% of the reactivity at this configuration ( $c_{01}^0 = 0.61$ , Table 2). We term this the (0,1) pathway, where the first value (0) gives the proton vibrational state of the neutral phenol–base and the second value is the state of the radical cation product. The (0,1) pathway is favored over the (0,0) path, which accounts for 25% of reactivity, and over pathways involving other excited states: (0,2), 7%; (1,0), 4%; and (2,0), 1%. The (0,1) path is favored because of its high vibrational overlap, that is,  $S_{01}^2 = 0.5 \gg S_{00}^2 = 0.008$ . In the cation, the ground-state ( $\nu = 0$ ) proton wave function is localized on the nitrogen, but the  $\nu = 1$  excited state has the proton delocalized over the oxygen and nitrogen, due to the highly anharmonic surface (Figure 1a; see also Figure 5 for example). In this case, the higher overlap is enough to overcome the general trend that transfers to excited states are disfavored because they are endoergic, for example,  $\Delta G_{01}^\circ = (\epsilon_1^1 - \epsilon_0^1) = +1352 \text{ cm}^{-1}$ . Pathways from vibrational excited states in the neutral reactant can be exoergic [e.g.,  $\epsilon_{\text{rel-}10} = (\epsilon_1^1 - \epsilon_0^0)_{\text{neutral}} = -1965 \text{ cm}^{-1}$ ] but are disfavored by the very low Boltzmann population of these states at 298 K. For instance, the population of the first excited state  $P_1$  in compound **1** is calculated to be  $8 \times 10^{-5}$ . Accessing excited vibrational states in the cations  $1^+ - 3^+$  is easier than in the neutrals because the cation surfaces are more anharmonic, and thus the vibrational energy spacings are smaller. This balancing of overlap, promotion energy, and  $\epsilon_{\text{rel-}\mu\nu}$  has been described by Hammes-Schiffer and co-workers in their development and applications of multistate continuum theory.<sup>26,27,29,31,33</sup>

For the phenol–CH<sub>2</sub>–pyridyl compound **2** and the phenol–amine **3**, the calculated CPET reaction profiles at TS<sub>0</sub> are similar to that of **1** (Table 2). Again, the (0,1) pathways are predicted to dominate CPET reactivity: 60% for **2** and 78% for **3**. The next most important pathways for **2** are (0,2) (33%) and (0,0) (6%), while for **3** they are (0,0) (17%) and (0,2) (5%).

The overall rate for each compound depends on the sum of all of the various pathways, which for these calculations at the TS<sub>0</sub> geometry is conveniently summarized as  $\zeta_0$  (eqs 8, 9). The values of  $\zeta_0$  for the three compounds are 0.0019 for **1**, 0.0002 for **2**, and

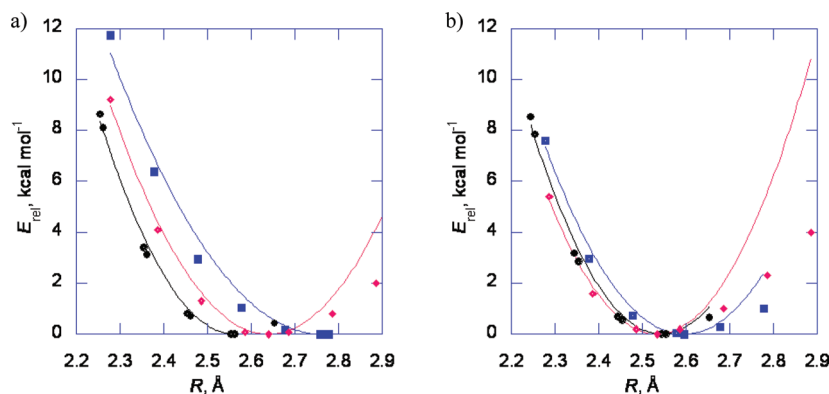
0.0045 for **3** (Table 2). Note that for each compound, the CPET reaction is dominated by the (0,1) pathway so the key terms are  $S_{01}^2$  and  $\epsilon_{\text{rel-}01}$ . Compound **3** has the highest value of  $\zeta_0$  because it has the most anharmonic proton surface in the radical cation (Figure 1). This anharmonicity not only increases the overlap for the 0 $\rightarrow$ 1 transition ( $S_{01}^2$ ), but it reduces the energy of the cation vibrational excited state ( $\epsilon_1^1$ ). The calculated trend in  $\zeta_0$  (**3** > **1** > **2**) mirrors the trend in the energy gap between the OH and NH minima on the radical cation surface, but not this energy gap in the neutral compounds (**1** < **3** < **2**). Therefore,  $\zeta_0$  appears to be more sensitive to the shape of the more anharmonic surface, in this case, the cation potential rather than the neutral hydrogen-bond potential.

This analysis at the TS<sub>0</sub> geometry has highlighted the importance of the shape of the hydrogen-bond potential in both the neutral and the cation. At this geometry, there are significant contributions from pathways from vibrational excited states. In the following section, this treatment will be extended to heavy atom configurations with varied proton donor–acceptor distances  $d_{\text{ON}}(R)$  to assess the impact of “promoting” vibrations along this coordinate.

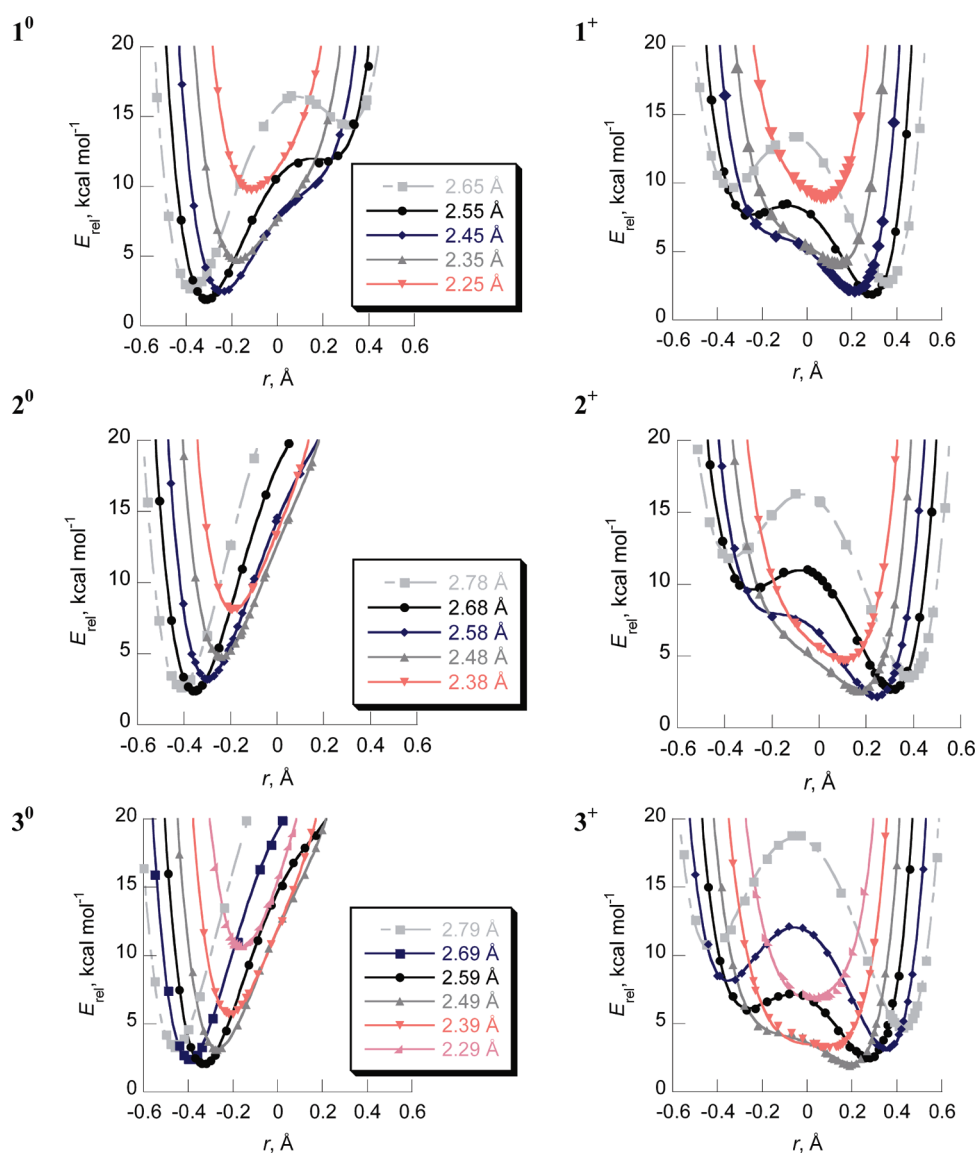
**IV. Effect of Compression along the R Coordinate.** The calculations above were all performed at the fixed TS<sub>0</sub> heavy-atom geometry. In solution, however, compounds **1–3** have a thermal population of various configurations. Of particular interest are configurations with different values of the O $\cdots$ N distance  $R$ . Such so-called “dynamical effects” are considered a critical parameter in proton transfer and PCET.<sup>15,17,18</sup> Motions along the  $R$  coordinate have been found to play a key role, for instance, in dynamical studies of PT in hydrogen-bonded systems,<sup>43,44</sup> as well as in enzymatic hydrogen atom and hydride transfers.<sup>18,24,45–48</sup>

The structures of **1–3** and their radical cations were optimized computationally with various fixed values of  $R$  to derive the potential energy along the O $\cdots$ N coordinate (Figure 3). This treatment has been shown to yield an effective force constant of donor–acceptor motions with contributions from all normal modes.<sup>33</sup> More emphasis was placed on  $R$  distances compressed from the TS<sub>0</sub> value because these configurations contribute more to the CPET rate (see below). The calculated energies as a function of  $R$  roughly fit parabolic surfaces, with effective force constants  $f = 176, 94$ , and  $137 \text{ kcal mol}^{-1} \text{ \AA}^{-2}$  for **1–3**. This trend in  $f$  is the inverse of the optimized  $R$  distances (**2** > **3** > **1**), with the –CH<sub>2</sub>–pyridine compound **2** having  $R$  more than 0.1 Å longer than those in **1** and **3**. In contrast, there is less variation in the force constants for the radical cations (183, 145, and  $174 \text{ kcal mol}^{-1} \text{ \AA}^{-2}$ ), where the optimized values of  $R$  are similar for **1**<sup>+</sup>–**3**<sup>+</sup>. Note, however, that in going to the cations, the force constants increase substantially more for compounds **2** and **3** than for **1**. This suggests that the primary factor determining the magnitude of the effective force constant along  $R$  is O $\cdots$ N steric repulsion, although the conjugation and resulting planarity of **1** may play a role.

CPET reactivity has been evaluated for **1–3** at several configurations, TS <sub>$R$</sub> , with varying values of  $R$ . Similar to TS<sub>0</sub>, these geometries are obtained from the average of the partially optimized geometries for the neutral and cationic species with  $R$  fixed at the indicated value. This procedure gives, to a reasonable approximation, structures with varying  $R$  along the multidimensional seam that separates the neutral reactant and cationic product. At each of these structures, the PT–PESs for the neutrals and cations have been calculated as described above and are shown in Figure 4. For each neutral and cationic compound,

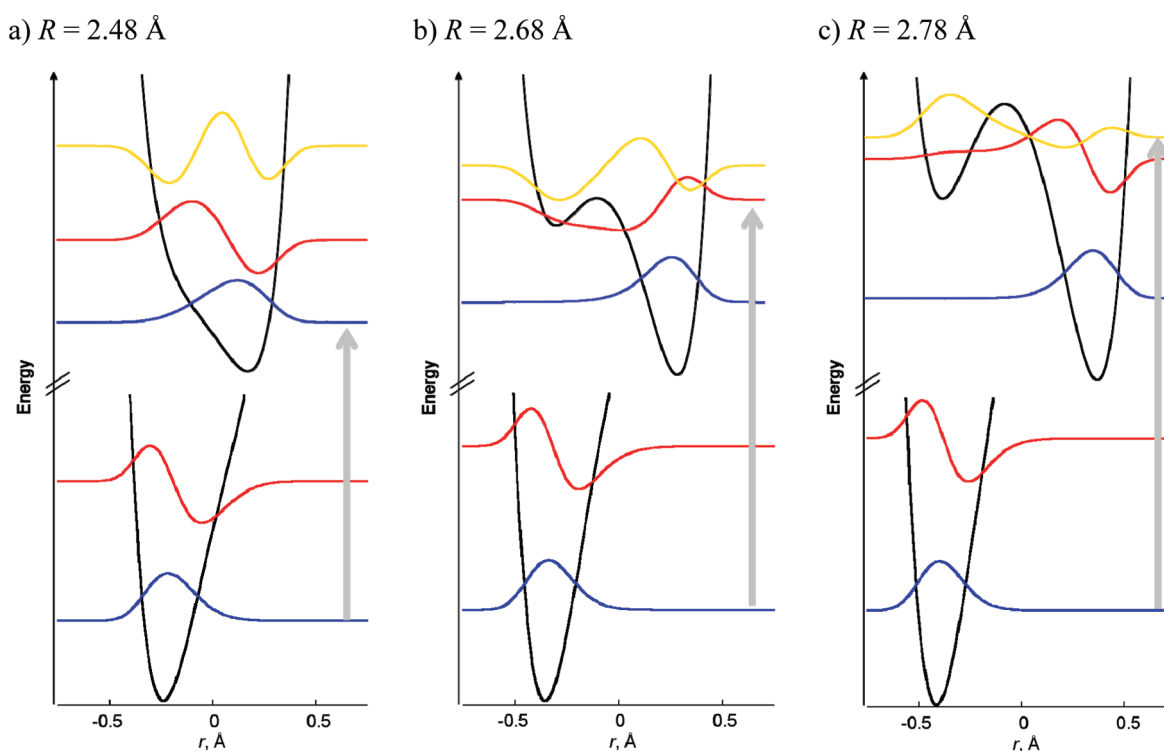


**Figure 3.** Variation of energy with  $R$  in 1 (●), 2 (blue ■), and 3 (red ◆) for (a) neutrals and (b) cations. The lines are parabolic fits ( $E_{\text{rel}} = 1/2f[R - R_{\text{min}}]^2$ ) of the points with  $R \leq R_{\text{min}}$ .



**Figure 4.** Computed proton potentials within the O–H–N hydrogen bonds at various  $\text{TS}_R$  configurations, for 1<sup>0</sup>–3<sup>0</sup> and 1<sup>+</sup>–3<sup>+</sup>.  $E_{\text{rel}}$  is the energy relative to the fully optimized geometry of each neutral or cation. In the PT coordinate, zero is the midpoint between the O and N atoms. Lines are fits to sixth-order polynomials. The  $R$  values indicated in the legends are the same for the neutral and the corresponding cation.





**Figure 5.** Hydrogen-bond potentials and proton wave functions for neutral **2** (below) and cationic **2**<sup>+</sup> (above). The wave functions are indicated with blue ( $\nu = 0$ ), red ( $\nu = 1$ ), and gold ( $\nu = 2$ ) lines. Gray arrows indicate the transition that dominates CPET reactivity at each heavy atom configuration. (a)  $\text{TS}_{2.48}$  ( $R = 2.48$  Å), the optimal configuration for CPET, where (0,0) is dominant and  $S_{0,0}^2 = 1.2 \times 10^{-1}$ ; (b)  $\text{TS}_0$  geometry,  $R = 2.68$  Å, where the (0,1) pathway dominates and  $S_{0,0}^2 = 3.8 \times 10^{-4}$ ; and (c)  $\text{TS}_{2.78}$  ( $R = 2.78$  Å), where (0,2) is dominant and  $S_{0,0}^2 = 2.5 \times 10^{-6}$ .

lengthening  $R$  leads to hydrogen-bond potentials with distinct wells corresponding to OH and NH forms, although the NH wells for **2**<sup>0</sup> and **3**<sup>0</sup> are shallow and high in energy. These wells are separated by a barrier, which increases in height with increasing  $R$ . Conversely, compression of  $R$  leads to more symmetric, single-well hydrogen-bond potentials with minima near the midpoint.

At each  $\text{TS}_R$  configuration, the proton vibrational energy levels and wave functions for **1–3** and **1**<sup>+</sup>–**3**<sup>+</sup> have been calculated and used to compute a value for  $\zeta_R$  (following eq 8 above). For configurations with shorter  $\text{O} \cdots \text{N}$  distances,  $\zeta_R$  is larger as anticipated due to the increasing overlap ( $S_{\mu\nu}^2$ ). In **1**, for example,  $S_{0,0}^2$  increases by nearly  $10^4$  as  $R$  decreases from 2.65 to 2.25 Å. Over these same configurations, however,  $\zeta_R$  increases by only a factor of 113, from 0.00038 to 0.043. This is due to the involvement of vibrational excited states at longer distances.

Figure 5 illustrates the involvement of vibrational excited states at varying values of  $R$  for **2**<sup>0</sup> and **2**<sup>+</sup>. At the  $\text{TS}_0$  configuration, where  $R = 2.68$  Å (Figure 5b), the  $\nu = 0$  vibrational levels for the neutral and the cation are both quite localized (i.e.,  $\text{OH} \cdots \text{N}$  and  $\text{O} \cdots \text{HN}$ , respectively) so  $S_{0,0}^2$  is very small. The dominant path is (0,1), as indicated by the gray arrow, because  $S_{0,1}^2$  is much larger due to the cation  $\nu = 1$  wave function having significant delocalization onto the oxygen. Increasing  $R$  by 0.1 Å to the  $\text{TS}_{2.78}$  geometry (Figure 5c) causes the  $\nu = 1$  state of the cation to become more localized on the nitrogen, and the transition with a large Franck–Condon factor is from the neutral  $\nu = 0$  to the cation  $\nu = 2$  states (gray arrow). However, this transition has a larger  $\varepsilon_{\text{rel-}\mu\nu}$ , making this less favorable. In contrast, compressing  $R$  to 2.48 Å causes the PT-PES to become much narrower and the neutral and cation  $\nu = 0$  wave functions have significant overlap,

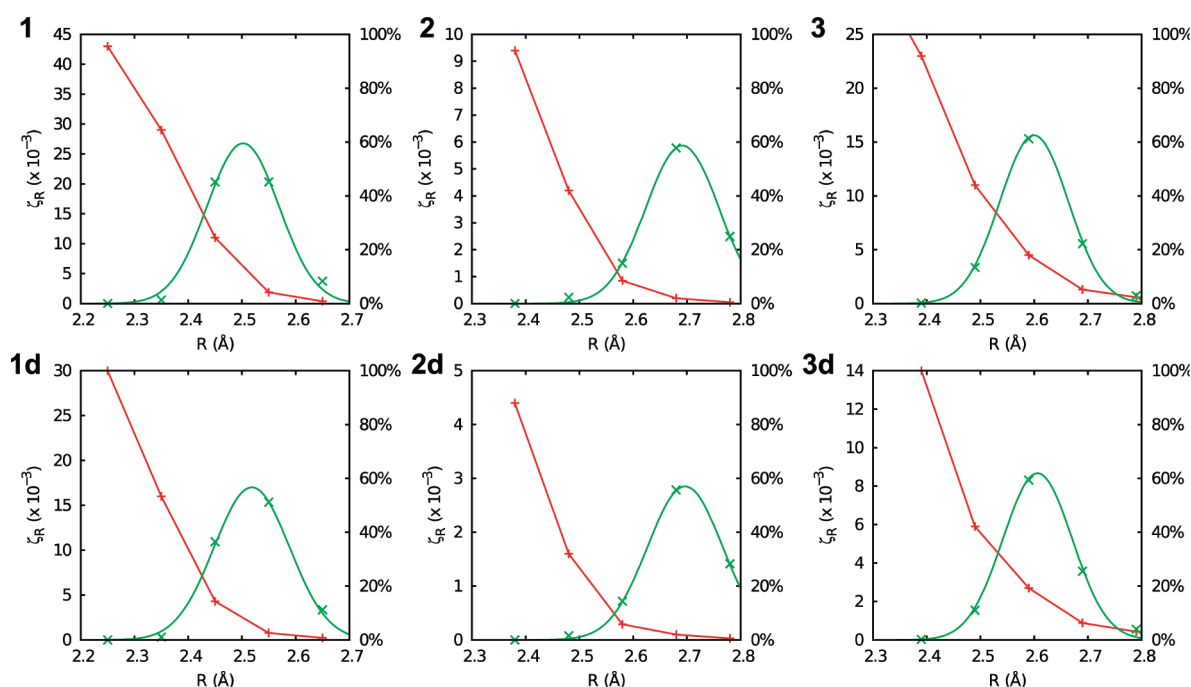
allowing this pathway to dominate (gray arrow in Figure 5a). These results are tabulated in detail for all compounds in the Supporting Information.

The overall CPET rate constant includes weighted contributions from each of these different  $R$  configurations. The rate expression is the same as eq 7 except that  $\zeta_0$  is replaced with a new parameter  $\zeta_{\text{tot}}$  reflecting the contribution of different  $R$  configurations, given by

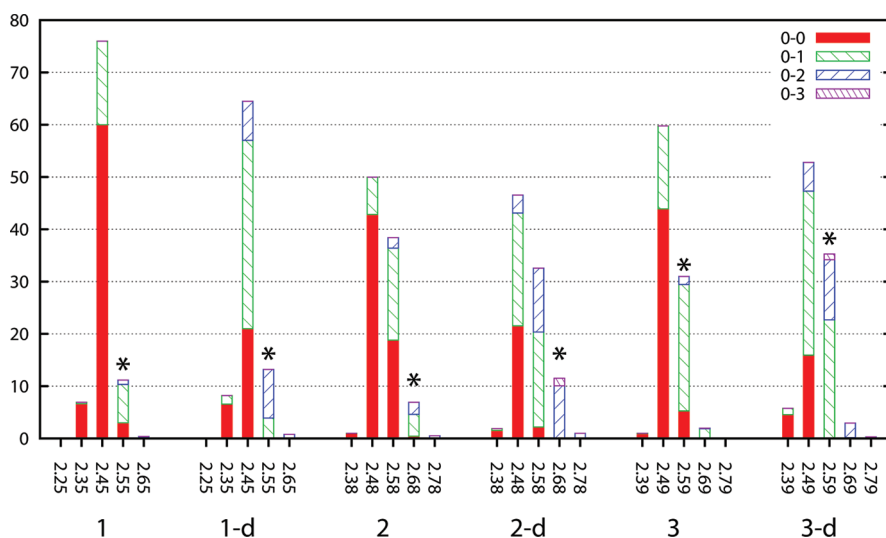
$$\zeta_{\text{tot}} = \sum_R P_R^1 \zeta_R \exp \left[ \frac{-(\text{IE}_R - \text{IE}_0)}{2k_B T} \right] \Delta R \quad (10)$$

where  $\zeta_R$  has the same form as  $\zeta_0$  (eq 8). Strictly speaking, this should be an integral over  $R$ , but our use of discrete configurations converts this to a sum with each configuration accounting for a reaction over a range  $\Delta R$ , reduced via division by 1 Å. Some additional discussion of the terms in this expression is warranted. The Boltzmann population of each  $R$  configuration ( $P_R^1$ ) not only includes the energy required to distort from  $\text{TS}_0$ , but also includes any changes in ZPE of the transferring proton (i.e.,  $\varepsilon_0$ ). The exponential term with  $\text{IE}_R$  accounts for the change in the ionization energy of each  $R$  configuration because conversions from the neutral to cation compounds are formally ionizations. The factor of 2 is required to relate the kinetics of CPET to the thermodynamics of ionization, because  $\Delta\Delta G^\ddagger / \Delta\Delta G^\circ \cong 1/2$  as discussed above. For compounds **2** and **3**, where the ground-state  $\text{O} \cdots \text{N}$  distance is substantially shorter in the cation versus the neutral (see Figure 3),  $\text{IE}_R$  is calculated to decrease substantially with  $R$ . For example, compressing  $R$  by 0.2 Å from  $\text{TS}_0$  lowers  $\text{IE}_R$  by 2.6 kcal mol<sup>−1</sup> (**2**) and 2.8 kcal mol<sup>−1</sup> (**3**) as compared to





**Figure 6.** Calculated  $\zeta_R$  (red +, left axis) and relative Boltzmann populations  $P_R$  (green ×, right axis) as a function of donor–acceptor distance  $R$  for 1–3 and the deuterio analogues 1d–3d. Green lines are normal distributions fit to  $P_R$ .



**Figure 7.** Contributions of  $R$  configuration and  $(\mu, \nu)$  pathways toward the total rate for compounds 1–3 and their deuterated analogues, with asterisks marking the  $TS_0$  configuration. Note that the most reactive configuration involves compression of  $R$ , and at this optimal configuration, the contribution from the (0,0) pathway increases.

$-0.5 \text{ kcal mol}^{-1}$  for 1. This energetic component of the “gating” action of promoting vibrations is a significant factor determining CPET reactivity, and one that has not been much emphasized.

Figure 6 shows a plot of both the calculated Boltzmann populations ( $P_R$ , green) and  $\zeta_R$  (red) as a function of  $R$ . While the maximum values of  $\zeta_R$  occur at shorter  $R$  values, as expected for better overlap between the neutral and cation  $\nu = 0$  wave functions, the  $P_R$ 's are centered near the  $TS_0$  distances. The net result is that the bulk of the CPET reactivity occurs at configurations with  $R$  compressed below  $TS_0$ ; this is shown in Figure 7 along with the various  $(\mu, \nu)$  pathways that contribute to each

configuration. For instance, the most likely  $R$  for CPET for 1 is computed to be 2.46 Å, which is 0.09 Å shorter than  $TS_0$ . At this compressed configuration, the (0,0) pathway dominates over the (0,1) pathway, which is opposite of that seen for the  $TS_0$  configuration (see also Table 2). Similar patterns of reactivity are computed for 2 and 3; that is, the increased  $\zeta_R$  values at shorter  $R$  are offset by the increasing energy required to reach the compressed configurations (the smaller thermal population). For 2, the most probable  $R$  for CPET is 2.52 Å, based on interpolation using a normal distribution, which is 0.17 Å shorter than  $TS_0$ . At this configuration, the (0,0) pathway dominates

**Table 3. Parameters Relevant to CPET Reactivity for Phenol–Bases 1–3 with Varied  $R^a$** 

system	$R$ at $TS_0$	$R^{†b}$	$E^{*c}$	$\zeta_0$	$\zeta_{tot}$	$\zeta_{tot,H}/\zeta_{tot,D}$
1	2.55	2.46	1.6	0.0019	0.0076	2.8
2	2.68	2.52	2.1	0.00020	0.0015	3.2
3	2.59	2.51	1.7	0.0045	0.0089	2.0

<sup>a</sup>Distances are in angstroms; energies are in kcal mol<sup>−1</sup>. <sup>b</sup> $R^\dagger$  indicates the optimal configuration for CPET; see text and Figure 6. <sup>c</sup> $E^*$  is the energy required to reach  $TS_0$  from optimized geometry of the neutral corrected for changes in ZPE.

with minor contributions from the (0,1) pathway. This indicates that for certain systems a simplified analysis including only vibrational ground states may be sufficient to capture some trends in reactivity.

This is again in contrast with the  $TS_0$  configuration where the (0,1) and (0,2) pathways dominate (60% and 30%, respectively). Surprisingly, the most probable  $R$  for **3** is 2.51 Å, a decrease of only 0.08 Å as compared to  $TS_0$ . This is very similar to the difference of 0.09 Å seen for **1** and likely reflects the difficulty of distorting compounds **1** and **3**, which have hydrogen bonds as part of a six-membered ring, as compared to compound **2** and its seven-membered ring. Finally, for the most reactive  $R$  configuration of **3** (i.e., 2.51 Å), the (0,0) pathway again dominates over the (0,1) pathway, which is opposite of that seen for the  $TS_0$  configuration. While the (0,0) pathway dominates at the  $TS_{peak}$  geometry, this transition accounts for only ca. 50% of the total reactivity of **3**. Similar conclusions can be reached for **1** and **2** where the (0,0) pathway is the largest contributor but excited states still play a significant role.

As presented in Table 3, the three structurally different compounds **1–3** give quite similar computed  $\zeta_{tot}$  values: 0.0076 (**1**), 0.0015 (**2**), and 0.0089 (**3**), which only vary by a factor of 5.9. This is remarkable in light of the almost 0.2 Å difference in the optimized  $R$  distances in the neutral phenol–bases (Table 1): 2.564 Å (**1**), 2.760 Å (**2**), and 2.640 Å (**3**). Typically, the molecule with the longer ground-state donor–acceptor distance is assumed to have a lower tunneling probability. For the compounds analyzed here, the similarity of the  $\zeta_{tot}$  values appears to be a result of the similarity of the transition structures  $TS_R$  at which CPET is most likely to occur, that is, compressed donor–acceptor distances with  $R = 2.45$ , 2.52, and 2.51 Å. If the proton is tunneling across roughly the same  $R$  distance in the three cases, then it is reasonable that the contributions of nuclear tunneling to the reactions will be similar.

Following the discussion above, with the assumptions that the solvent reorganization energies  $\lambda_{out}$  and the electronic coupling elements  $V^{el}$  are the same for the three phenols, the relative theoretical rate constants between **1**, **2**, and **3** are simply given by the relative  $\zeta_{tot}$  values. The computed rate constants reproduce the experimental trend that the pyridine derivative **1** reacts faster than its  $CH_2py$  analogue **2**.<sup>12</sup> Quantitatively, the computed factor of 5 difference is in only modest agreement with the experimental factor of ca. 10<sup>2.49</sup>. Much poorer agreement is seen for the computations involving the amine derivative **3**, which is computed to be as reactive as **1** but is experimentally seen to be similar to **2**.<sup>10</sup>

The mixed agreement between experiment and theory could have a number of origins, as a variety of simplifying assumptions have been necessary to apply multistate continuum theory (eq 2) to these CPET reactions. The averaged TS geometries

may contain strained bond lengths or angles that lead to nonphysical effects in the computation of the energies required to distort along the  $R$  coordinate, although this does not appear to be a major factor here.<sup>50</sup> Further, the  $R$  coordinate motion has been treated classically, and the proton potential surfaces are calculated with fixed heavy-atom positions, in a Born–Oppenheimer-type separation. A more complete treatment would involve coupling of these modes; however, this would probably not remedy a 100-fold discrepancy. Because the agreement is reasonable when comparing the two pyridyl derivatives, this suggests that the amine **3** may not be as similar to the pyridine compounds as has been assumed. The  $-CPh_2NH_2$  substituent in **3** is somewhat larger than the  $-py$  and  $-CH_2py$  groups in **1** and **2** and is not aromatic, so  $\lambda_{out}$  and  $V^{el}$  may be significantly different for **3**.  $V^{el}$  likely differs among compounds **1–3** due to differences in sterics around the phenol, which could lead to a significant decrease in the rates of **3** in which the phenol is protected by the *gem*-diphenyl groups. Additionally, delocalization of the redox active molecular orbital in **1** could lead to an increase in  $V^{el}$ . Finally, solvation, which is not included in this treatment, could influence the shape of the cation potential energy surfaces and therefore  $\zeta_{tot}$  because of the involvement of vibrational excited states. Preliminary calculations using a polarized continuum model (PCM) with the optical dielectric constant of MeCN suggest that  $\zeta_0$  for **3** is reduced by a factor of  $\sim 3$  relative to  $\zeta_0(1)$ , making  $\zeta_0(3)_{PCM} \cong \zeta_0(1)_{PCM}$ . Thus, this is not a dramatic effect. Solvation likely has the greatest influence on **3**<sup>+</sup> because of the higher localization of charge on the  $sp^3$  (as opposed to  $sp^2$ ) nitrogen atom. These issues together likely account for much of the discrepancy between experiment and theory in the comparison of **1** and **3**.

It is interesting to note that better quantitative agreement is obtained from a purely energetic analysis, putting aside the detailed multistate continuum theory computations. The energy to proceed from the optimized geometry of the neutral ground state to the most probable CPET configuration ( $TS_{R^\dagger}$ ) is 1.7, 4.0, and 2.6 kcal mol<sup>−1</sup> for **1**, **2**, and **3**, respectively. All other things being equal, these would correspond to relative rate constants of 49:1:11, in modest agreement with the  $1 > 2 \approx 3$  trend observed experimentally. We have previously derived crude estimates of intrinsic barriers using a model adapted from Nelsen’s four-point method,<sup>51</sup> which treats the proton classically and incorporates the energy of PT into the inner-sphere reorganization energy. While this is an incomplete model and the computed barriers do not quantitatively agree with experiment, the calculations do predict that **2** and **3** should react with higher intrinsic barriers as compared to **1**. Thus, in both the multistate continuum model and the simple four-point method, the relative barrier heights match those found experimentally.

These computational results are an interesting contrast with recent unimolecular flash-quench kinetic studies by Hammarström and co-workers on a series of phenol base compounds, including analogues of **1** and **2**, tethered to a  $Ru(bpy)_3^{2+}$  photosensitizer.<sup>5f</sup> They found differences in reactivity similar to those derived from our stopped-flow measurements. In their study, they found a strong empirical correlation between PCET reactivity and crystallographic values of  $R$ , which lead to the conclusion that proton tunneling distance was a key factor in determining rates. However, this relationship has not been observed in other related studies on phenol oxidations.<sup>5e,52</sup> In the present study with its focus on proton tunneling, including the effects of donor–acceptor motions and various vibrational states, a strong distance dependence

is not observed. Comparing the two phenol–pyridines, the present treatment does predict slower rates for **2**, which has a longer proton donor–acceptor distance. However, this difference is the result of a combination of factors, including not only tunneling probabilities between vibrational ground states, but also differences in anharmonicity of the hydrogen-bond potentials, variations in ionization energy with distance, and the energy required to reach more reactive configurations. The presence of these various factors suggests that changes in proton transfer distances influence PCET reactions of hydrogen-bonded systems in multiple and sometimes competing ways.

**V. Effects of Deuterium Substitution.** The analysis above has also been done for a transferring deuteron instead of a proton, in compounds **1d**, **2d**, and **3d**. The increased mass of the deuteron leads to more localized  $\nu = 0$  wave functions and decreased energetic spacing in the vibrational levels. The more localized wave functions result in smaller  $S_{\mu\nu}^2$  factors for the (0,0) pathways for **1d**–**3d**; this along with the closer energetic spacing of the vibrational levels leads to larger contributions from pathways involving excited states. For example, in **1d** at  $TS_0$ , the (0,0) pathway is predicted to account for only 1% of CPET reactivity, as compared to 25% for the proteo analogue (Table 2). Note that the Boltzmann populations of the  $\nu = 1$  states in the neutrals are still predicted to be very small, for instance,  $5 \times 10^{-4}$  in neutral **1d**, and so most of the effect arises from the changes in the cation wave functions. The optimal CPET configuration for both **1** and **1d** has  $R$  compressed by 0.1 Å as compared to  $TS_0$  (i.e., 2.46 Å). However, at this  $TS_R$  structure, the (0,1) pathway dominates for **1d** (48%) as compared to only 28% for the (0,0) pathway, while for **1** the pattern is reversed with 75% and 20% for the (0,0) and (0,1) pathways, respectively (Figure 7). It is interesting to note that  $\zeta_{H,R}/\zeta_{D,R}$  decreases as  $R$  is lengthened beyond  $TS_0$ .<sup>52</sup> This counterintuitive result is in line with our recent report comparing **3** and an analogue with an increased proton transfer distance, which displays lower experimental KIEs.<sup>53</sup> This effect is predicted because the pathways to excited states, which are favored at longer  $R$ , are more accessible in the deuterio analogues due to their closer energetic spacing of the vibrational excited states. Still, deuterium substitution has only minor effects on the average  $TS_R$  populations and contributions to CPET. Similar results are obtained from analysis of **2d** and **3d**; that is, there is little change in the reactive donor–acceptor distance, but the reactivity has greater contributions from the pathways involving cation excited states.

These results can be compared to those found experimentally using the assumption that  $V^{\text{el}}$  and  $\lambda$  are independent of deuteration, which allows the ratio  $\zeta_{\text{tot,H}}/\zeta_{\text{tot,D}}$  to be used as an approximation for the KIE. For **1**,  $\zeta_{\text{tot,H}}/\zeta_{\text{tot,D}} = 2.8$  (Table 3), which is in excellent agreement with the experimental values observed in the solution reactions of **1/1d** ( $R = {}^t\text{Bu}$ ) with various  $[\text{Fe}(\text{R}_2\text{bpy})_3]^{3+}$  oxidants, 2.5–2.9.<sup>10b</sup> Similar agreement is found for **3**:  $\zeta_{\text{tot,H}}/\zeta_{\text{tot,D}}$  is calculated to be 2.0, again within the range of experimental  $k_{\text{H}}/k_{\text{D}}$  values of 1.6–2.6 for oxidations of **3/3d** ( $R = {}^t\text{Bu}$ ,  $R' = \text{Ph}$ ).<sup>10b</sup> For **2**, the experimental KIE for the oxidation by  $[\text{Fe}(\text{S,S'}\text{-Me}_2\text{bpy})_3]^{3+}$  is  $5.9 \pm 0.8$ , larger than the values of 2.5 and 2.6 measured for **1** and **3** ( $R = {}^t\text{Bu}$ ) with the same oxidant.<sup>10,12</sup> The calculated  $\zeta_{\text{tot,H}}/\zeta_{\text{tot,D}}$  for **2** = 3.2 is significantly smaller than the experimental value, but is larger than that of **1** or **2**, in line with the experimental trend. Direct comparison of  $\zeta_{\text{tot,H}}/\zeta_{\text{tot,D}}$  and KIE is complicated by the fact that the KIE can vary with  $\Delta G^\circ$  to different degrees in these phenol–base systems.<sup>53</sup> Therefore, while this treatment does

not totally capture the larger KIE observed for an oxidation of **2**, the predictions of moderate primary isotope effects for oxidations of **1**–**3** are in agreement with experiment.

This computational methodology can also be used to calculate the variation of the kinetic isotope effect with temperature. Experimentally, the  $k_{\text{H}}/k_{\text{D}}$  for the oxidation of **2** and **2d** by  $[\text{Fe}(\text{S,S'}\text{-Me}_2\text{bpy})_3]^{3+}$  decreases from 6.1 to 3.4 over a 50 °C range (278–328 K).<sup>12</sup> Arrhenius analysis of the data gave  $E_{\text{a,H}} - E_{\text{a,D}} = 2.3 \pm 1.2 \text{ kcal mol}^{-1}$  and  $\log(A_{\text{H}}/A_{\text{D}}) = -1.0 \pm 0.8$ .<sup>12</sup> These values appear to be outside of the semiclassical limits, that is,  $E_{\text{a,H}} - E_{\text{a,D}} > 1.1 \text{ kcal mol}^{-1}$  and  $\log(A_{\text{H}}/A_{\text{D}}) < -0.15$ ,<sup>54</sup> and therefore we previously suggested that nuclear quantum effects are playing a role.<sup>12</sup> With the assumption that the shape of the surfaces, wave functions, and their energies are independent of temperature,  $\zeta_{\text{tot}}$  has been computed for proteo and deuterio **2** at 278 K ( $\zeta_{\text{tot,H}} = 1.03 \times 10^{-3}$ ,  $\zeta_{\text{tot,D}} = 2.85 \times 10^{-4}$ ) and 328 K ( $\zeta_{\text{tot,H}} = 2.34 \times 10^{-3}$ ,  $\zeta_{\text{tot,D}} = 8.61 \times 10^{-4}$ ). In agreement with experiment,  $\zeta_{\text{tot,H}}/\zeta_{\text{tot,D}}$  decreases in going from 298 K (3.6) to 328 K (2.7). Fitting  $\zeta_{\text{tot}}$  versus  $T$  data to the Arrhenius equation gives  $E_{\text{a,H}} - E_{\text{a,D}} = 1.03 \text{ kcal mol}^{-1}$ , which is smaller than the experimental value, while the computed ratio of Arrhenius  $A$  factors,  $\log(A_{\text{H}}/A_{\text{D}}) = -0.25$ , is in agreement with the experimental number. These calculations thus support the suggestion that the observation of  $A_{\text{H}}/A_{\text{D}} < 1$  is an experimental marker for systems where tunneling occurs from configurations with decreased distance.<sup>45</sup>

**VI. Mechanistic Implications.** The mechanisms of many proton/electron transfer reactions have typically been discussed in terms of stepwise versus concerted transfer of the two particles. The one-electron oxidations of **1**–**3** could in principle proceed by initial proton transfer (PT) to give a zwitterionic species  $^-\text{OAr}-\text{BH}^+$  that would then undergo electron transfer (ET), or by initial ET to give a phenol radical cation  $\text{HOAr}^{+\bullet}-\text{B}$  that would subsequently undergo PT. In previous reports,<sup>10–12</sup> we have shown that the experimental estimates of minimum energies for these potential intermediates are too high for them to be involved in the reaction chemistry observed. Thus, a concerted (one-step) transfer of the proton and electron, CPET, is indicated in each case. The primary kinetic isotope effects (KIE) observed and the variation of rates with driving force ( $\Delta\Delta G^\ddagger/\Delta\Delta G^\circ_{\text{CPET}} \approx 0.5$ ) provide additional evidence for this pathway.<sup>1,5,10–12</sup>

The calculations described here provide a more detailed look at the nature of these mechanisms. Attempts to locate minima corresponding to the potential intermediates  $^-\text{OAr}-\text{BH}^+$  and  $\text{HOAr}^{+\bullet}-\text{B}$  at this level of theory have been unsuccessful. Indeed, the calculated vibrational wave functions for the neutrals suggest that the PT intermediate  $^-\text{OAr}-\text{BH}^+$  is not possible because there are no wave functions localized on the N atom. Similarly, for the cations, the excited vibrational wave functions are never localized on the O atom. Therefore, it seems that in compounds with strong hydrogen bonds, such as these phenol–bases, concerted may be the only option because there are no well-defined states corresponding to the stepwise intermediates.

The vibrational wave functions, such as those in Figure 5, allow an even closer look at the CPET reactions of **1**–**3**. All three compounds, at the proton donor–acceptor distance  $R^\ddagger$  that is most likely for CPET, have the same most important single pathway. This pathway involves electron transfer simultaneous with proton tunneling from the ground vibrational state of the neutral, with the proton localized on oxygen, to the ground vibrational state of the cation, in which H is predominantly on



nitrogen (Table 2). This is the traditional picture of a concerted proton–electron transfer.

The full picture of the CPET process is, however, more complicated. CPET occurs over a range of donor–acceptor distances  $R$  (Figure 7), and the qualitative shape of the vibrational wave functions and the major pathways are strong functions of  $R$  (Figure 4). For instance, at the  $TS_0$  structure for **2**, the dominant pathway is calculated to involve CPET from the vibronic ground state of the neutral, where the proton is OH bound, to a vibrational excited state in the cation where the proton is delocalized across the hydrogen bond (Figure 5b). Even at the most probable CPET distance  $R^\ddagger$ , 14–26% of the reaction occurs via this pathway. When  $R$  is compressed below  $R^\ddagger$ , the proton wave functions for both the neutral and the cation become centered close to the midpoint of the hydrogen bond (Figures 4 and 5). In this situation, the proton is not localized at either the O or the N, and the concept of a binary “proton transfer” is not meaningful.

At the other extreme, when  $R$  is elongated, the hydrogen-bond potential of the cations develops a double-well topology with a large barrier separating OH and NH wells (see Figure 4). This double-well potential gives nearly degenerate pairs of vibrational states localized on the oxygen and nitrogen. For example, the  $\nu = 2$  state in  $2^+$  with  $R = 2.78$  Å is predominantly localized on the oxygen (Figure 5c). At this value of  $R$ , the dominant CPET pathway (93%) is from the O–H localized  $\nu = 0$  state in the neutral  $2^0$  to this primarily O–H localized  $\nu = 2$  excited state in  $2^+$ . In this model, with  $R$  fixed at 2.78 Å, ET occurs with very little change in the proton position, the OH to NH motion occurring by subsequent vibrational relaxation in the cation. This situation of CPET with little movement of the proton bears resemblance to the recent experiments reported by Meyer and co-workers where optical intramolecular ET in phenolic dye molecules is coupled to intermolecular proton transfer to a hydrogen-bonded base. While proton motion on the time scale of optical ET is forbidden by the Franck–Condon principle, a portion of the dye molecules yield a vibrationally excited state where the proton remains located near the donor but bonded to the acceptor as indicated by coherent Raman experiments.<sup>8c</sup> CPET is concerted in the sense of not having a stable intermediate, but on a microscopic level it involves electron transfer with little instantaneous proton transfer. The decreased  $\zeta_H/\zeta_D = 1.3$  computed at the  $TS_0$  configuration is consistent with this picture.

The picture of the CPET oxidations that emerges from these calculations is therefore more subtle than the stepwise versus concerted mechanistic dichotomy. While all of the pathways are concerted in the sense of not proceeding through a long-lived intermediate, a small fraction of ( $\sim 0.5\%$ ) the reaction of **2**, for instance, is calculated to proceed by quasi vertical ionization from the optimized geometry of the neutral ( $R = 2.76$  Å) to yield a vibrationally excited state of the cation in which the proton is still mostly localized on the oxygen. This is a very minor pathway because the energy to remove the electron at this optimized neutral geometry is 9.5 kcal mol<sup>−1</sup> higher than the ionization energy of  $TS_0$ . This is a microscopic view of the argument we (and others) have made that the higher thermodynamic cost of ET/PT pathway often outweighs its lower intrinsic barrier.<sup>5,10</sup> With **1** and **3**, there is also a very minor vertical ionization pathway, but in these cases, the  $\nu = 1$  wave function in the cation product has more density in the NH well, making the distinction between “ET” and “CPET” less clear, even for this one transition.

It should be emphasized that the very large majority of the reactivity of **1–3** is calculated to proceed with substantial distortion of the heavy atom framework from the ground state to more reactive configurations. This inner-sphere reorganization involves both distortion toward the cation structure, thereby lowering the energy to remove an electron, and compression of the proton donor–acceptor distance to facilitate proton tunneling to the product state (which may or may not look like a complete transfer of H). The need for heavy-atom movement prior to hydrogen transfer has, as noted above, been emphasized in a number of other studies.<sup>18,24,45</sup> Our experimental results on these reactions have also implicated a substantial inner-sphere reorganization energy because CPET reactions of **1–3** are substantially slower than pure electron transfer reactions of similarly sized organic reagents (comparisons in the same solvent and at similar driving force).<sup>10–12</sup>

## CONCLUSIONS AND CLOSING COMMENTS

Differences in concerted proton–electron transfer (CPET) reactivity observed for phenol–base compounds **1–3** have been probed using a version of multistate continuum theory. In this model, the proton is treated as a quantum mechanical particle, and motions along the proton donor–acceptor ( $R$ ) coordinate are included. The parameters that contribute to CPET can be summarized as: energy-weighted Franck–Condon overlaps of accessible proton vibrational states for the reactant (neutral) and product (cation), modulation of the energetics of ET with changes in  $R$  ( $\Delta E_R$ ), and the energetics required to reach reactive configurations. With simplifying assumptions (some derived from experimental data), all of the necessary parameters have been computed using DFT and other calculations; no adjustable or fixed parameters have been used.

All three reactions are predicted to have optimal values of  $R$  for CPET between 2.46 and 2.51 Å. This is a surprising result because the optimized ground-state geometries have values of  $R$  that vary much more widely, from 2.56 to 2.76 Å. CPET reactivity is modestly higher (by factors of 2–7.5) when  $R$  is contracted by 0.1–0.2 Å below the transition structures, that is, the average of the ground-state neutral and cation structures. Changes in  $R$  have substantial qualitative effects on the proton potential energy surfaces, proton vibrational wave functions, and the overlaps between vibrational wave functions. For these strongly hydrogen-bonded systems, Morse potentials are not a good approximation. For all three compounds, the dominant pathway for CPET at the optimal value of  $R$  primarily involves the ground-state vibrational levels, with a minor contribution from the cation  $\nu = 1$  state. However, at configurations with longer  $R$ , and for the deuterated analogues, CPET pathways from the vibrational ground state in the neutral to vibrational excited states in the cation are predicted to dominate. These pathways are viable in **1–3** because of the highly anharmonic hydrogen-bond potentials of the cationic species, a contrast with systems such as C–H oxidation reactions. Analyses of the various pathways reveal a more complex picture than the classical stepwise versus concerted dichotomy for proton/electron transfer reactions.

This analysis has mixed success in reproducing experimental results. The theory mostly captures the experimentally observed kinetic isotope effects, and the relative reactivity of the  $-\text{py}$  and  $-\text{CH}_2\text{py}$  derivatives. The reactivity of the amine compound **3**, however, is not well predicted. Some of the discrepancies may result from the simplifications needed in the computational



work, such as computing smaller molecules in the gas phase rather than the full system in MeCN solution, as well as assumptions regarding the relative reorganization energies  $\lambda$  and the electronic coupling matrix elements  $V^{\text{el}}$ .

The analysis presented here indicates that an interplay of energetic barriers and quantum mechanical effects of the proton transfer affect CPET reactivity. The importance of pathways to or from vibrationally excited states is of interest and seems to explain the recent counterintuitive observation in one system of decreased KIE with increased proton transfer distance.<sup>53</sup> This work may also provide experimentally testable predictions. For example, in the limit of  $2\lambda \gg |\Delta G^\circ|$ , Marcus models predict  $\Delta\Delta G^\ddagger/\Delta\Delta G^\circ = 0.5$ , but significant contributions of pathways to excited product states should lead to  $\Delta\Delta G^\ddagger/\Delta\Delta G^\circ > 0.5$ .<sup>8b,14,17</sup> Experimental studies to further probe these issues in CPET reactivity are ongoing.

## ■ ASSOCIATED CONTENT

**S Supporting Information.** Complete ref 35, Cartesian coordinates of optimized structures, and additional details on the calculations. This material is available free of charge via the Internet at <http://pubs.acs.org>.

## ■ AUTHOR INFORMATION

### Corresponding Author

\*E-mail: [tmarkle@u.washington.edu](mailto:tmarkle@u.washington.edu) (T.F.M.), [mayer@chem.washington.edu](mailto:mayer@chem.washington.edu) (J.M.M.).

### Present Addresses

<sup>†</sup>Department of Photochemistry and Molecular Science, Uppsala University, Box 523, S-75120 Uppsala, Sweden.

## ■ ACKNOWLEDGMENT

We are grateful to the U.S. National Institutes of Health for grant GM50422 and an ARRA supplement, and to the University of Washington for support of this work. The U.S. National Science Foundation (NSF-CRIF Grant CHE-0342956) provided support for the computational resources used. We especially thank Dr. Eric Heatwole, Andri Arnaldsson, and Prof. Oleg Prezhdo for sharing their program to calculate vibrational wavefunctions from sixth-order polynomial surfaces, and Prof. Xiaosong Li for computational assistance and insightful discussions.

## ■ REFERENCES

- (1) (a) Huynh, M. H. V.; Meyer, T. J. *Chem. Rev.* **2007**, *107*, 5004–5064. (b) Mayer, J. M. *Annu. Rev. Phys. Chem.* **2004**, *55*, 363–390. (c) Hodgkiss, J. M.; Rosenthal, J.; Nocera, D. G. In *Hydrogen-Transfer Reactions*; Hynes, J. T., Klinman, J. P., Limbach, H.-H., Schowen, R. L., Eds.; Wiley-VCH: Weinheim, 2006; pp 503–562. (d) Cukier, R. I.; Nocera, D. G. *Annu. Rev. Phys. Chem.* **1998**, *49*, 337–369. (e) Costentin, C. *Chem. Rev.* **2008**, *108*, 2145–2179. **2010**, *110*, PR1–40.
- (2) The term CPET was coined by: Costentin, C.; Evans, D. H.; Robert, M.; Savéant, J.-M.; Singh, P. S. *J. Am. Chem. Soc.* **2005**, *127*, 12490–12491.
- (3) (a) Meyer, T. J.; Huynh, M. H. V.; Thorp, H. H. *Angew. Chem., Int. Ed.* **2007**, *46*, 5284–5304. (b) Umena, Y.; Kawakami, K.; Shen, J.-R.; Kamiya, N. *Nature* **2011**, *473*, 55–61. (c) Barry, B. A. *J. Photochem. Photobiol., B* **2011**, *104*, 60–71.
- (4) (a) Biczók, L.; Gupta, N.; Linschitz, H. *J. Am. Chem. Soc.* **1997**, *119*, 12601. (b) Gupta, N.; Linschitz, H. *J. Am. Chem. Soc.* **1997**, *119*, 6384.
- (5) (a) Sjödin, M.; Styring, S.; Wolpher, S.; Xu, Y.; Sun, L.; Hammarström, L. *J. Am. Chem. Soc.* **2005**, *127*, 3855–3863. (b) Sjödin, M.; Irebo, T.; Utlas, J. E.; Lind, J.; Merényi, G.; Åkermark, B.; Hammarström, L. *J. Am. Chem. Soc.* **2006**, *128*, 13076–13083. (c) Irebo, T.; Reece, S. Y.; Sjödin, M.; Nocera, D. G.; Hammarström, L. *J. Am. Chem. Soc.* **2007**, *129*, 15462–15464. (d) Irebo, T.; Johansson, O.; Hammarström, L. *J. Am. Chem. Soc.* **2008**, *130*, 9194–9195. (e) Johannissen, L. O.; Irebo, T.; Sjödin, M.; Johansson, O.; Hammarström, L. *J. Phys. Chem. B* **2009**, *113*, 16214–16225. (f) Zhang, M.-T.; Irebo, T.; Johansson, O.; Hammarström, L. *J. Am. Chem. Soc.* **2011**, *133*, 13224–13227.
- (6) Reece, S. Y.; Nocera, D. G. *J. Am. Chem. Soc.* **2005**, *127*, 9448–9458.
- (7) (a) Costentin, C.; Robert, M.; Savéant, J.-M. *J. Am. Chem. Soc.* **2006**, *128*, 8726–8727. (b) Costentin, C.; Robert, M.; Savéant, J.-M. *J. Am. Chem. Soc.* **2007**, *129*, 9953–9963. (c) Correction to ref 7b: Costentin, C.; Robert, M.; Savéant, J.-M. *J. Am. Chem. Soc.* **2010**, *132*, 2845. (d) Bonin, J.; Costentin, C.; Louault, C.; Robert, M.; Routier, M.; Savéant, J.-M. *Proc. Natl. Acad. Sci. U.S.A.* **2010**, *107*, 3367–3372.
- (8) (a) Fecenko, C. J.; Meyer, T. J.; Thorp, H. H. *J. Am. Chem. Soc.* **2007**, *128*, 11020. (b) Fecenko, C. J.; Thorp, H. H.; Meyer, T. J. *J. Am. Chem. Soc.* **2007**, *128*, 15098–15099. (c) Westlake, B. C.; Brenneman, M. K.; Concepcion, J. J.; Paul, J. J.; Bettis, S. E.; Hampton, S. D.; Miller, S. A.; Lebedeva, N. V.; Forbes, M. D. E.; Moran, A. M.; Meyer, T. J.; Papanikolas, J. M. *Proc. Natl. Acad. Sci. U.S.A.* **2011**, *108*, 8554–8558.
- (9) (a) Moore, G. F.; Hambourger, M.; Gervald, M.; Poluektov, O. G.; Rajh, T.; Gust, D.; Moore, T. A.; Moore, A. L. *J. Am. Chem. Soc.* **2008**, *130*, 10466. (b) Moore, G. F.; Hambourger, M.; Kodis, G.; Michl, W.; Gust, D.; Moore, T. A.; Moore, A. L. *J. Phys. Chem. B* **2010**, *114*, 14450.
- (10) (a) Rhile, I. J.; Mayer, J. M. *J. Am. Chem. Soc.* **2004**, *126*, 12718–12719. (b) Rhile, I. J.; Markle, T. F.; Nagao, H.; DiPasquale, A. G.; Lam, O. P.; Lockwood, M. A.; Rotter, K.; Mayer, J. M. *J. Am. Chem. Soc.* **2006**, *128*, 6075–6088.
- (11) Markle, T. F.; Rhile, I. J.; DiPasquale, A. G.; Mayer, J. M. *Proc. Natl. Acad. Sci. U.S.A.* **2008**, *105*, 8185–8190.
- (12) Markle, T. F.; Mayer, J. M. *Angew. Chem., Int. Ed.* **2008**, *47*, 738–740.
- (13) Benisvy, L.; Bittl, R.; Bothe, E.; Garner, C. D.; McMaster, J.; Ross, S.; Teutloff, C.; Neese, F. *Angew. Chem., Int. Ed.* **2005**, *44*, 5314–5317.
- (14) (a) Marcus, R. A.; Sutin, N. *Biochim. Biophys. Acta* **1985**, *811*, 265–322. (b) Barbara, P. F.; Meyer, J. T.; Ratner, M. A. *J. Phys. Chem.* **1996**, *100*, 13148–13168.
- (15) (a) Keifer, P. M.; Hynes, J. T. In *Hydrogen-Transfer Reactions*; Hynes, J. T., Klinman, J. P., Limbach, H.-H., Schowen, R. L., Eds.; Wiley-VCH: Weinheim, 2006; pp 303–348. (b) Antoniou, D.; Basner, J.; Nunez, S.; Schwartz, S. D. *Chem. Rev.* **2006**, *106*, 3170–3187.
- (16) Krishtalik, L. I. *Biochim. Biophys. Acta* **2000**, *1458*, 6–27.
- (17) (a) Hammes-Schiffer, S. In *Hydrogen-Transfer Reactions*; Hynes, J. T., Klinman, J. P., Limbach, H. H., Schowen, R. L., Eds.; Wiley-VCH: Weinheim, 2007; pp 479–503. (b) Hammes-Schiffer, S.; Stuchebrukhov, A. A. *Chem. Rev.* **2010**, *110*, 6939–6960.
- (18) Pu, J.; Gao, J.; Truhlar, D. G. *Chem. Rev.* **2006**, *106*, 3140–3169.
- (19) (a) Reference 17. (b) Hammes-Schiffer, S. *J. Phys. Chem. Lett.* **2011**, *2*, 1410–1416. (c) Sirjoosingh, A.; Sharon Hammes-Schiffer, S. *J. Phys. Chem. A* **2011**, *115*, 2367–2377 and refs 23–33. (d) Iyengar, S. S.; Sumner, I.; Jakowski, J. *J. Phys. Chem. B* **2008**, *112*, 7601–7613. (e) Kamerlin, S. C. L.; Warshel, A. *J. Phys. Org. Chem.* **2010**, *23*, 677–684. (f) Hay, S.; Johannissen, L. O.; Sutcliffe, M. J.; Scrutton, N. S. *Biophys. J.* **2010**, *98*, 121–128. (g) Boekelheide, N.; Salomón-Ferrer, R.; Miller, T. F., III. *Proc. Nat. Acad. Sci. U.S.A.* **2011**, *108*, 16159–16163.
- (20) (a) Clary, D. C. *Science* **2008**, *321*, 789–791. (b) Iyengar, S. S.; Sumner, S.; Jakowski, J. *J. Phys. Chem. B* **2008**, *112*, 7601–7613.

- (21) For a small sample of recent examples, see: (a) Siegbahn, P. E. M.; Blomberg, M. R. A. *Chem. Rev.* **2010**, *110*, 7040–7061. (b) Shaik, S.; Kumar, D.; de Visser, S. P.; Altun, A.; Thiel, W. *Chem. Rev.* **2005**, *105*, 2279–2328. (c) Derat, E.; Shaik, S. *J. Am. Chem. Soc.* **2006**, *128*, 13940–13949. (d) DiLabio, G. A.; Ingold, K. U. *J. Am. Chem. Soc.* **2005**, *127*, 6693–6699. (e) Louwse, M. J.; Vassilev, P.; Baerends, E. J. *J. Phys. Chem. A* **2008**, *112*, 1000–1012. (f) Wang, Z.-C.; Xue, W.; Ma, Y.-P.; Ding, X.-L.; He, S.-G.; Dong, F.; Heinbuch, S.; Rocca, J. J.; Bernstein, E. R. *J. Phys. Chem. A* **2008**, *112*, 5984–5993. (g) A perspective with both adiabatic and non-adiabatic treatments is given in: Tishchenko, O.; Truhlar, D. G.; Ceulemans, A.; Nguyen, M. T. *J. Am. Chem. Soc.* **2008**, *130*, 7000–7010.
- (22) In addition, for these particular reactions involving aminium ions, the electronic couplings  $V^{\text{el}}$  may be quite small, based on the values for the sterically similar self-exchange ET of these reagents: Nelsen, S. F.; Weaver, M. N.; Luo, Y. *J. Phys. Chem. A* **2006**, *110*, 11665–11676.
- (23) Soudackov, A.; Hatcher, E.; Hammes-Schiffer, S. *J. Chem. Phys.* **2005**, *122*, 014505.
- (24) (a) Hatcher, E.; Soudackov, A. V.; Hammes-Schiffer, S. *J. Am. Chem. Soc.* **2004**, *126*, 5763–5775. (b) Hatcher, E.; Soudackov, A. V.; Hammes-Schiffer, S. *J. Am. Chem. Soc.* **2007**, *129*, 187–196.
- (25) Skone, J. H.; Soudackov, A. V.; Hammes-Schiffer, S. *J. Am. Chem. Soc.* **2006**, *128*, 16655–16663.
- (26) Iordanova, N.; Hammes-Schiffer, S. *J. Am. Chem. Soc.* **2002**, *124*, 4848–4856.
- (27) Ludlow, M. K.; Soudackov, A. V.; Hammes-Schiffer, S. *J. Am. Chem. Soc.* **2009**, *131*, 7094–7102.
- (28) Ludlow, M. K.; Soudackov, A. V.; Hammes-Schiffer, S. *J. Am. Chem. Soc.* **2010**, *132*, 1234–1235.
- (29) Iordanova, N.; Decornez, H.; Hammes-Schiffer, S. *J. Am. Chem. Soc.* **2001**, *123*, 3723–3733.
- (30) Carra, C.; Iordanova, N.; Hammes-Schiffer, S. *J. Am. Chem. Soc.* **2003**, *125*, 10429–10436.
- (31) Ishikita, H.; Soudackov, A. V.; Hammes-Schiffer, S. *J. Am. Chem. Soc.* **2007**, *129*, 11146–11152.
- (32) Hazra, A.; Soudackov, A. V.; Hammes-Schiffer, S. *J. Phys. Chem. B* **2010**, *114*, 12319–12332.
- (33) Auer, B.; Fernandez, L. E.; Hammes-Schiffer, S. *J. Am. Chem. Soc.* **2011**, *133*, 8282–8292.
- (34) The bulk of this study was done concurrently with ref 5e. Markle, T. F. Ph.D. Thesis, University of Washington, 2009.
- (35) Frisch, M. J.; et al. *Gaussian 03*, revision D.02; Gaussian, Inc.: Pittsburgh, PA, 2004. See the Supporting Information for a complete citation.
- (36) (a) Basilevsky, M. V.; Rostov, I. V.; Newton, M. D. *Chem. Phys.* **1998**, *232*, 189–199. (b) Newton, M. D.; Rostov, I. V.; Basilevsky, M. V. *Chem. Phys.* **1998**, *232*, 201–210. (c) Basilevsky, M. V.; Chudinov, G. E.; Rostov, I. V.; Liu, Y.-P.; Newton, M. D. *J. Mol. Struct.* **1996**, *371*, 191–203.
- (37) Heatwole, E.; Arnaldsson, A.; Prezhdo, O., unpublished work.
- (38) The assumption that the transition structure (TS) is halfway between the reactant **A** and the products **A<sup>+</sup>** is, in the Marcus picture, equivalent to the ubiquitous assumption that a single force constant and  $\lambda$  can be used to describe the curvature of both the reactant and the product parabolas. This assumption has been shown to introduce a very small error even when the force constants of **A** and **A<sup>+</sup>** are significantly different. (a) Newton, T. W. *J. Chem. Educ.* **1968**, *45*, 571–575. See also: (b) Marcus, R. A. *J. Chem. Phys.* **1965**, *43*, 679 (Appendix IV). (c) Marcus, R. A. *Faraday Symp. Chem. Soc.* **1975**, *10*, 60. (d) For a treatment of the reduced force constant, see: Sutin, N. *Prog. Inorg. Chem.* **1983**, *30*, 441–498, especially p 452.
- (39) Instead of assuming that the proton moves on a surface defined by fixed heavy atoms, the alternative limiting approximation is to assume that all of the nuclear motions occur on the same timescale, which yields adiabatic vibrational surfaces and normal modes (see Supporting Information Figure S1). The differences in these two approaches have been discussed in detail for *ortho*-hydroxyaryl ketimines: Filarowski, A.; Koll, A.; Hansen, P. E.; Kluba, M. *J. Phys. Chem. A* **2008**, *112*, 3478–3485.
- (40) Manner, V. W.; Markle, T. F.; Freudenthal, J. H.; Roth, J. P.; Mayer, J. M. *Chem. Commun.* **2008**, 256–258.
- (41) Using the freq=anharmonic keyword in Gaussian 03, see: Barone, V. *J. Chem. Phys.* **2005**, *122*, 014108.
- (42) Bratos, S.; Leicknam, J.-C.; Gallot, G.; Ratajczak, H. In *Ultrafast Hydrogen Bonding Dynamics and Proton Transfer Processes in the Condensed Phase*; Elsaesser, T., Bakker, H. J., Eds.; Kluwer Academic: Boston, 2002; pp 5–30.
- (43) Fontaine-Vive, F.; Johnson, M. R.; Kearley, G. J.; Howard, J. A. K.; Parker, S. F. *J. Am. Chem. Soc.* **2006**, *128*, 2964–2969.
- (44) Jerzierska, A.; Panek, J. *J. Chem. Theory Comput.* **2008**, *4*, 375–384.
- (45) (a) Klinman, J. P. *Biochim. Biophys. Acta* **2006**, *1757*, 981–987. (b) Klinman, J. P. *Chem. Phys. Lett.* **2009**, 179–193.
- (46) Liu, B.; Warshel, A. *J. Phys. Chem. B* **2007**, *111*, 7852–7861.
- (47) (a) Masgrau, L.; Roujeinikova, A.; Johannissen, L. O.; Hothi, P.; Basran, J.; Ranaghan, K. E.; Mulholland, A. J.; Sutcliffe, M. J.; Scrutton, N. S.; Leys, D. *Science* **2006**, *312*, 237. (b) Johannissen, L. O.; Hay, S.; Scrutton, N. S.; Sutcliffe, M. J. *J. Phys. Chem. B* **2007**, *111*, 2631–2638. (c) Hay, S.; Sutcliffe, M. J.; Scrutton, N. S. *Proc. Natl. Acad. Sci. U.S.A.* **2007**, *104*, 507. (d) Pudney, C. R.; Johannissen, L. O.; Sutcliffe, M. J.; Hay, S.; Scrutton, N. S. *J. Am. Chem. Soc.* **2010**, *132*, 11329–11335. (e) Peters, B. *J. Chem. Theory Comput.* **2010**, *6*, 1447–1454. (f) Benkovic, S. J.; Hammes-Schiffer, S. *Science* **2003**, *301*, 1196–1202.
- (48) Nagel, Z. D.; Klinman, J. P. *Chem. Rev.* **2010**, *110*, PR41–PR67.
- (49) Apparent deviations from the Marcus cross relation have been observed experimentally in the reactions of compound **1**. Therefore, depending on the oxidant used, rate constants for **1** are a factor of ca. 25–250 times greater than those of **2**.<sup>10b,12</sup>
- (50) Using  $E_R$  values derived from the force constant for compression along the *R* coordinate in neutral **1–3** has only minor effects on the values of  $\zeta_{\text{tot}}$ .
- (51) (a) Nelsen, S. F.; Blackstock, S. C.; Kim, Y. *J. Am. Chem. Soc.* **1987**, *109*, 677. (b) Nelsen, S. F.; Weaver, M. N.; Pladziewicz, J. R.; Ausman, L. K.; Jentzsch, T. L.; O’Konek, J. J. *J. Phys. Chem. A* **2006**, *110*, 11665–11676.
- (52) This behavior is predicted for configurations where pathways to excited states predominate. In contrast,  $\zeta_{\text{H,R}}/\zeta_{\text{D,R}}$  is predicted to increase with longer distance *R* when the (0,0) pathway dominates.
- (53) Markle, T. F.; Rhile, I. J.; Mayer, J. M. *J. Am. Chem. Soc.* **2011**, *133*, 17341–17352.
- (54) Bell, R. P. *The Tunnel Effect in Chemistry*; Chapman and Hall: New York, 1980; pp 77–105.